Symmetry-recovering crises of chaos in polarization-related optical bistability

M. Kitano, T. Yabuzaki, and T. Ogawa
Radio Atmospheric Science Center, Kyoto University, Uji, Kyoto 611, Japan
(Received 21 September 1983)

We investigate delay-induced chaos in an optically bistable system which has a symmetry with respect to the exchange of two circular polarizations. Roughly speaking, the output of the system bifurcates in the following way as the input light intensity increases: (1) symmetric steady state, (2) asymmetric steady state, (3) asymmetric periodic oscillation, (4) asymmetric chaos, and (5) symmetric chaos. The first bifurcation is a well-known symmetry-breaking transition. It is shown that the last bifurcation through which the symmetry is recovered can be viewed as a crisis of chaos, which has been defined by Grebogi *et al.* as a sudden change of strange attractor. By changing system parameters, we find three distinct types of the crises in the experiment with an electronic circuit which simulates the difference-differential system equation. Before and after the crises, waveforms characteristic of each type are observed. In a simple two-dimensional-map model, we can find all three types of crises. It is also found that the types of crises are determined by the nature of unstable fixed (or periodic) points which cause the crises by colliding with the chaotic attractors. The symmetry-recovering crises seem to be general phenomena appearing in nonlinear systems with some symmetries.

I. INTRODUCTION

The phenomenon of chaos has been the subject of intense interest in the last few years. It is now recognized as a common phase of the nonlinear dynamical system in addition to the conventional phases of stationary equilibrium and periodic (or quasiperiodic) oscillation. Since Ikeda *et al.*[1] have predicted chaotic behaviors in an optically bistable system, many theoretical and experimental studies have been made.[2–5] An optical system is a suitable method with which to study nonlinear phenomena including chaos because it has tractable theoretical models and precise experiments are possible. If necessary, we can add moderate complexities to it.[6,7] Along this line, we have proposed an optical system which utilizes interactions between right and left circularly polarized light beams through a $J=\frac{1}{2}$ to $J=\frac{1}{2}$ transition.[8] We have shown that symmetry breaking and optical tristability are possible for this system. Since then, various kinds of phenomena have been predicted[4,9] and some of them have been demonstrated experimentally.[10]

Recently, we proposed a new version of such a polarization-related bistable system that utilizes the optically induced Faraday effect and needs no optical cavity.[11] We also performed the experiment by using a sodium cell and a multimode dye laser tuned to a wing of the D_1 line.[12] An interesting feature of the system is that it exhibits the most typical pitchfork bifurcation which breaks the polarization symmetry. Namely, the symmetry-breaking bifurcation is of a supercritical type, while in the tristable system[8] it is of a subcritical type. In this paper we investigate the delay-induced chaos in this optical system. When we increase the input light intensity passing over the first bifurcation, a chaotic state having polarization asymmetry appears. If we increase the intensity still more, fully developed symmetric chaos is reached. We are thus interested in the bifurcation which lies between those two states. As we will see later, the symmetry recovering occurs through a sudden change of the chaotic attractors. Recently, Grebogi *et al.*[13] have introduced a new class of bifurcation named "crises of chaos," where the size of chaotic attractor suddenly changes. We will show that in our case the symmetry is recovered through the crisis.

In Sec. II, we show the setup of the system and derive the system equation which is a one-dimensional difference-differential equation having symmetry with respect to the exchange of two circular polarizations. In Sec. III, we discuss a one-dimensional-map model and show a simple example of symmetry-recovering crisis. In Sec. IV, we describe the experimental setup of an electronic circuit to simulate the optical system. In the experiment we observe three distinct types of symmetry-recovering crises. In Sec. V, we introduce a two-dimensional-map model to explain the experimental results. Although the model seems to be oversimplified to approximate our system in infinite-dimensional space, it can reproduce all three types of crises. We present the strange attractors near crises for each type, and discuss how they recover the symmetry. As we will see, unstable fixed points play important roles in crises. So we show the classification of fixed points of the two-dimensional map in an appendix. Finally, we summarize our results and discuss the remaining questions.

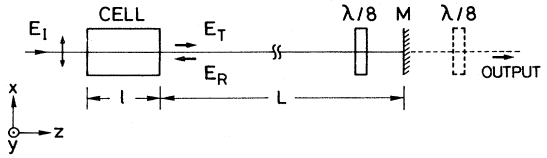

FIG. 1. Schematic illustration of the optically bistable system without an optical cavity.

II. SYSTEM EQUATION

We consider an optically bistable system shown in Fig. 1. It is largely the same as the one in Refs. 11 and 12 except that a delay in the feedback is introduced by taking a large distance L between the cell and the mirror M. Following the model adopted for the previous studies,[8,11,12] we consider spin-$\frac{1}{2}$ atoms which are optically pumped by the incident and the reflected light beams which are tuned to the wing of the resonance line. The state of the ensemble of atoms can be characterized by the magnetization component M_z along the optical axis, which is proportional to the population difference between $m_J=\frac{1}{2}$ and $m_J=-\frac{1}{2}$ sublevels in the ground state. The time evolution of M_z is described by the Bloch equation:

$$\frac{dM_z}{dt}=-(\Gamma+I_+ +I_-)M_z+(I_+ -I_-)M_0 , \tag{1}$$

where Γ is the relaxation rate of the magnetization and $I_\pm$ are the $\sigma_\pm$ light intensities which are normalized so as to give pumping rates. If I_+ (I_-) is large enough compared to I_- (I_+) and Γ, all atoms are oriented along the $+z$ ($-z$) direction and the maximum polarization $M_z=M_0$ ($-M_0$) is attained.

The absorption coefficients $\alpha_\pm$ and the wave number $k_\pm$ for $\sigma_\pm$ light are determined by the normalized magnetization component $m_z=M_z/M_0$ as

$$\alpha_\pm=\alpha(1\mp m_z) , \tag{2}$$

$$k_\pm=k_0+\kappa(1\mp m_z) , \tag{3}$$

where α and κ are the absorption coefficient and the incremental wave number for the unpolarized ($m_z=0$) medium, respectively, and k_0 is the wave number in a vacuum. In the dispersion regime we can neglect the absorption losses.

The polarization plane of the linearly polarized incident light is rotated by an angle θ when the difference between k_+ and k_- exists (Faraday rotation). If we represent the incident light field as $\vec{E}_I=\sqrt{I_0}\hat{x}$, the transmitted field $\vec{E}_T$ is given by

$$\vec{E}_T=\sqrt{I_0}(\hat{x}\cos\theta+\hat{y}\sin\theta) , \tag{4}$$

$$\theta(t)=(k_- -k_+)l/2=m_z(t)\kappa l , \tag{5}$$

where l is the length of the cell and $\hat{x}$ and $\hat{y}$ are the unit vectors.

The transmitted light is reflected by the mirror M set at a distance L and is fed back to the cell. Thus, the feedback is delayed by the amount $t_R=2L/c$. In the feedback path, a $\lambda/8$ plate is inserted whose optic axis is oriented to the x axis. By its action, the polarization state of the light fed back to the cell becomes

$$\vec{E}_R=\sqrt{I_{R+}}\hat{e}_- -\sqrt{I_{R-}}\hat{e}_+ , \tag{6}$$

$$I_{R\pm}=RI_0\{1\pm\sin[2\theta(t-t_R)]\}/2 , \tag{7}$$

where $\hat{e}_\pm=(-\hat{x}\pm i\hat{y})/\sqrt{2}$ and R is the reflectivity of the mirror. The $\sigma_\pm$ components of the reflected light suffer complementary modulations according to $\sin2\theta(t-t_R)$. Experimentally, the polarization state of $\vec{E}_R$ can be observed by monitoring the output light transmitting through the mirror M and an auxiliary $\lambda/8$ plate. We can also monitor the polarization state $\vec{E}_T$ by setting the fast axes of two $\lambda/8$ plates to form right angles. From Eqs. (7) and (5) we have the light intensities in the cell:

$$I_\pm=I_0\{1\pm R\sin[2\kappa l m_z(t-t_R)]\} . \tag{8}$$

Substitution of Eq. (8) into Eq. (1) gives the system equation as follows:

$$dm_z/dt=-(\Gamma+2I_0)m_z(t)+RI_0\sin[2\kappa l m_z(t-t_R)] . \tag{9}$$

Changing the time scale by

$$t'=\gamma^{-1}(\Gamma+2I_0)t$$

and introducing a new variable

$$X(t')=2\kappa l m_z(t) ,$$

we have a normalized form:

$$\gamma^{-1}\frac{dX}{dt'}=-X(t')+\mu\sin[X(t'-t_R')] , \tag{10}$$

where $\mu=2\kappa lRI_0/(\Gamma+2I_0)$ and

$$t_R'=\gamma^{-1}(\Gamma+2I_0)t_R .$$

In the case $\Gamma\gg I_0$, μ is proportional to I_0 and t_R' is independent of I_0. In the experiment we can vary $t_R'\gamma$ by changing the length L or the relaxation rate Γ. Hereafter, we drop the primes in t' and t_R'. When $t_R\gamma=0$, Eq. (10) is an ordinary differential equation in one dimension, while in the limit $t_R\gamma\gg1$, the system can be described by a difference equation as described in Sec. III. Therefore, the parameter $t_R\gamma$ represents whether Eq. (10) is close to a difference equation or to a differential equation.

Note that Eq. (10) is invariant under the transformation $X\rightarrow -X$, which corresponds to the exchange of the roles of the spin-up and -down atoms and the right and left circularly polarized light.

III. ONE-DIMENSIONAL-MAP MODEL

In the limiting case $t_R\gamma\gg1$, we can formally reduce Eq. (10) to the difference equation:

$$X_{n+1}=\mu\sin X_n , \tag{11}$$

which defines an iteration of the one-dimensional map. As is well known,[2,3,14] this equation gives an adequate qualitative prediction for the bifurcation structure for Eq. (10) with $t_R\gamma\gg1$.

Figure 2 shows the bifurcation diagram for Eq. (11). For $\mu<\mu_0=1$, there exists only one stable fixed point: $X=0$. At $\mu=\mu_0$ a pitchfork bifurcation occurs at which the solution $X=0$ becomes unstable and a symmetry-breaking transition takes place. This symmetry breaking can also be seen for the case $t_R\gamma=0$.[11,12] In Fig. 2 we showed only the negative branch after the bifurcation. As μ increases, each asymmetric branch undergoes period doublings followed by chaos. For $\mu<\mu_{(0)}$, the chaotic orbit is confined to the regions $X>0$ or $X<0$, namely, the output state is chaotic but still elliptically polarized to either direction. At $\mu=\mu_{(0)}$, the chaotic band suddenly doubles its width. There the two oppositely polarized

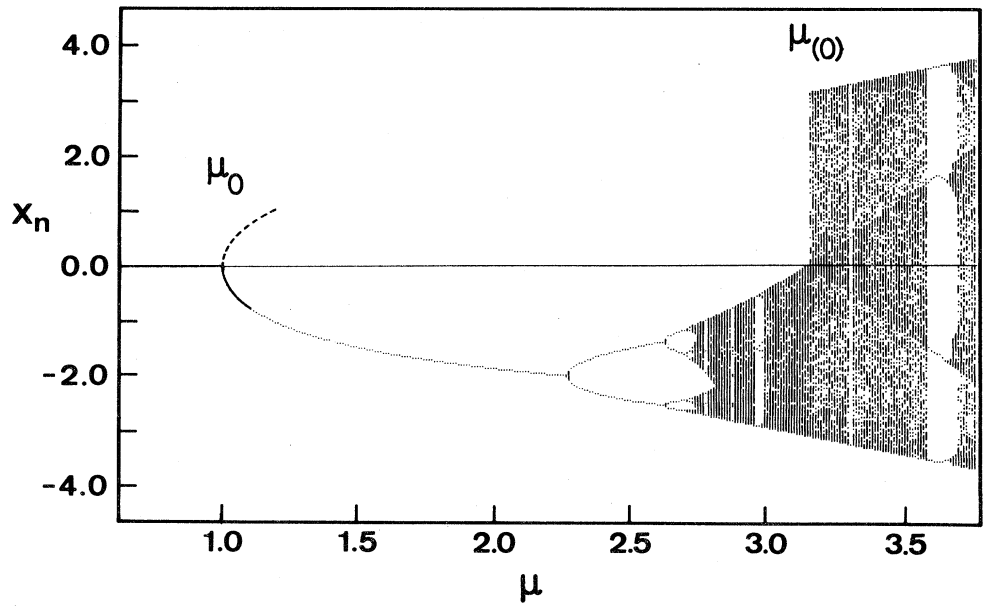

FIG. 2. Bifurcation diagram for the map, Eq. (11). For a given value of μ, an initial point is chosen and its orbit is plotted after preiteration to avoid transient phenomena. The same procedure is repeated for a slightly increased value of μ where the last point is used as the initial value. At $\mu=\mu_0=1$, a symmetry-breaking bifurcation occurs. For $\mu>\mu_0$, only the negative branch is pictured. The positive branch can be obtained by the transformation $X\rightarrow -X$. At $\mu=\mu_{(0)}$, a symmetry recovering is seen.

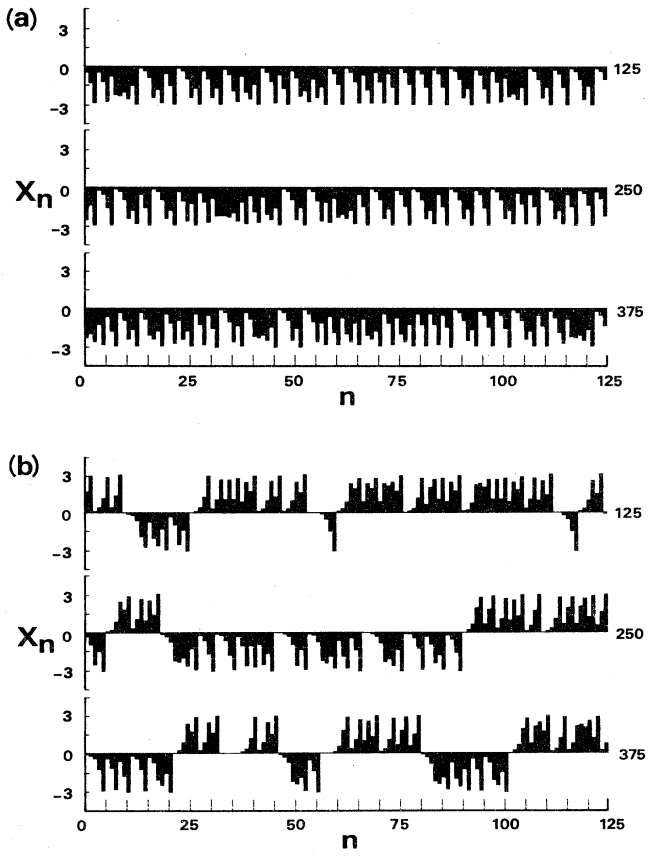

FIG. 3. Waveforms of Eq. (11) for (a) $\mu=3.11$ (before the crisis) and (b) $\mu=3.17$ (after the crisis). Bar graph of X_n as a function of n for 375 iterations after preiteration.

bands collide to form a single band. Thus, the symmetry broken at $\mu=\mu_0$ is recovered at $\mu=\mu_{(0)}$.

The sudden change may be viewed as the crisis of chaos named by Grebogi *et al.*[13] The crisis occurs when a strange attractor collides with a coexisting unstable fixed point or periodic orbit. In our case the situation is somewhat degenerate due to the symmetry, namely, a strange attractor collides with an unstable fixed point $X=0$ and the other coexisting strange attractor simultaneously. We call the phenomenon "symmetry-recovering crisis."

Figures 3(a) and 3(b) show examples of chaotic orbits for cases before ($\mu\lesssim\mu_{(0)}$) and after ($\mu\gtrsim\mu_{(0)}$) the crisis. The short-time behaviors are the same for both cases but, in the latter, crossover to the other polarized state sometimes occurs. According to Ref. 13, the average lifetime τ_{av} of each polarized state is estimated as

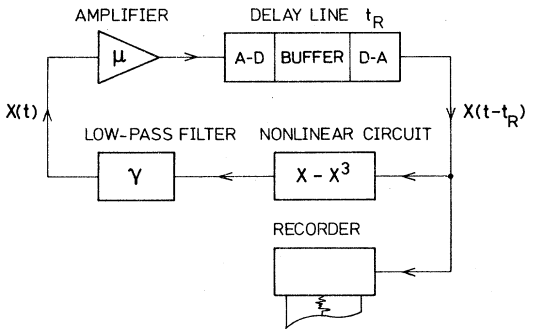

FIG. 4. Experimental setup. The analog circuit simulates the difference-differential equation (10).

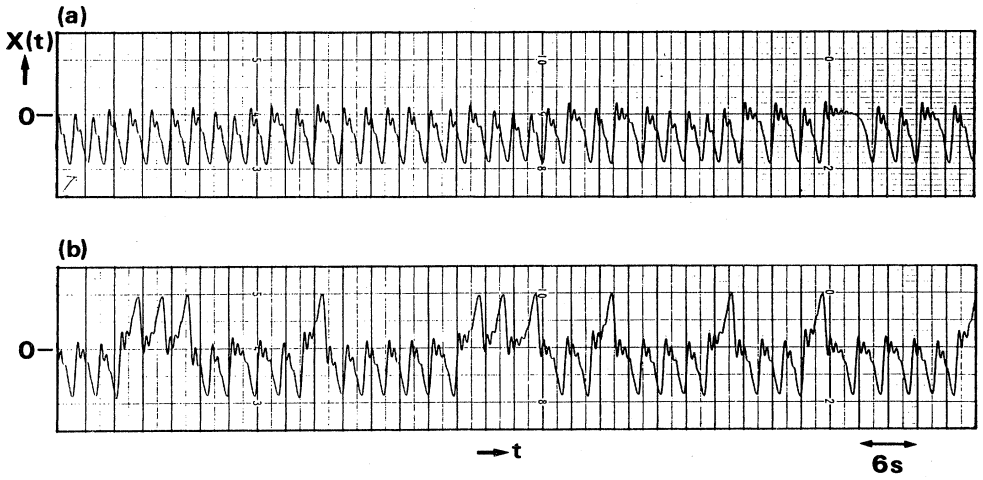

FIG. 5. Waveforms (a) before and (b) after the symmetry-recovering crisis of type I. Parameters: $t_R=0.41$ s, $\gamma=2.0$ Hz, (a) $\mu=4.26$; (b) $\mu=4.38$.

$$\tau_{\text{av}}\sim(\mu-\mu_{(0)})^{-1/2}\ . \tag{12}$$

We confirmed the estimation numerically.

IV. SIMULATION BY ANALOG CIRCUIT

In order to see how the symmetry-recovering crises for Eq. (10) appear we constructed an analog circuit which simulates Eq. (10). Figure 4 shows the experimental set-up. The nonlinear function $\sin X$ in Eq. (10) is approximated by $X-X^3$ and realized by two analog multipliers (Intersil ICL8013) and an operational amplifier. The delay t_R is given by a digital delay line equipped with a 12-bit (binary digit) analog-to-digital (A-D) converter, a digital-to-analog (D-A) converter, and a 4096-word buffer. The cutoff frequency γ of the low-pass filter is set at 2 Hz when we record waveforms on a strip chart recorder. We can conveniently find bifurcation points or crises on a cathode-ray tube (CRT) instead of the recorder by setting $\gamma\sim10^2$–10^3 Hz and shortening t_R correspondingly.

By changing t_R, we could find three distinct types of symmetry-recovering crises. We named them type I, II, and III according to the order of the values t_R for which each type was observed. The critical value $\mu_{(0)}$ for crisis decreases as $t_R\gamma$ increases.

Type I. Before the crisis, rather regular pulsing is observed [Fig. 5(a)]. We can see damped oscillations near $X=0$ between the pulses, whose durations are different from pulse to pulse. Such oscillation is not observed when μ is far below $\mu_{(0)}$ and appears as μ approaches $\mu_{(0)}$. After the crisis [Fig. 5(b)], the crossover to the other polarized state neccessarily occurs through the damped oscillation. Thus, the oscillation may be viewed as a precursor for the crisis and also as a crossover transient.

Type II. The waveform before the crisis [Fig. 6(a)] is fairly random. The bursts of periodic oscillation are precursors for the crisis. They appear randomly and their duration is also random. After the crisis [Fig. 6(b)], the crossover occurs through the burst of oscillation.

Type III. At a glance there seems to be no difference

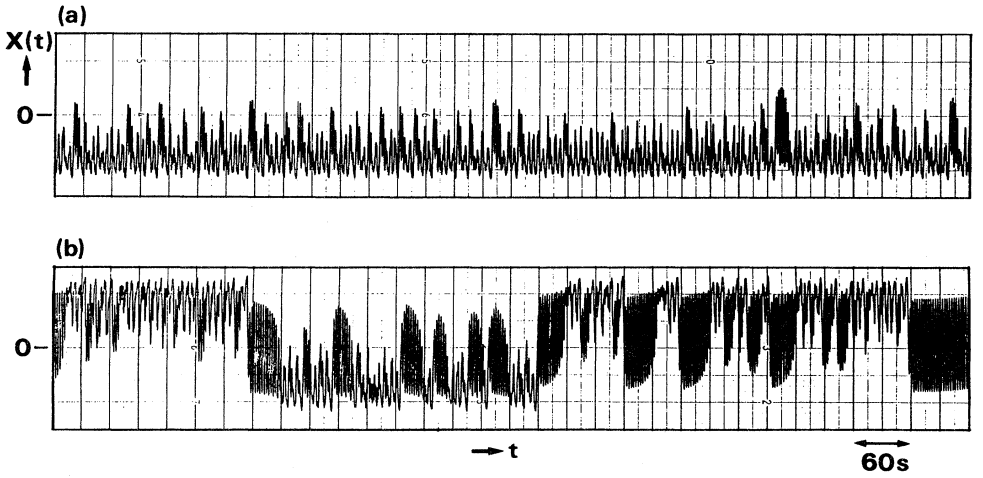

FIG. 6. Waveforms (a) before and (b) after the type II crisis. Parameters: $t_R=2.05$ s, $\gamma=2.0$ Hz, (a) $\mu=2.96$; (b) $\mu=3.02$.

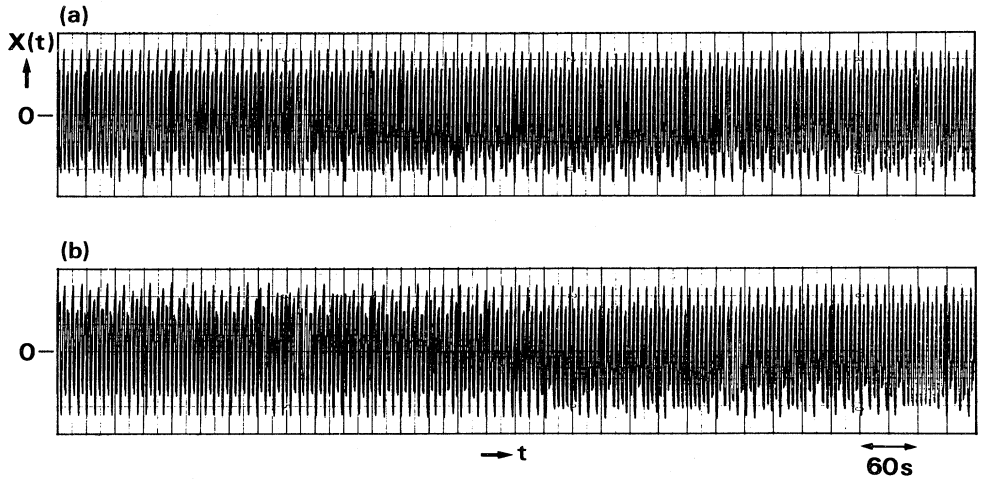

FIG. 7. Waveforms (a) before and (b) after the type III crisis. Parameters: $t_R=4.10$ s, $\gamma=2.0$ Hz, (a) $\mu=2.77$; (b) $\mu=2.79$.

between Figs. 7(a) and 7(b). However, the waveform in Fig. 7(a) shows period-4 chaos which has an asymmetry with respect to X; the upper boundary is flat while the lower is not. In the middle of Fig. 7(b) we can see a crossover. No marked precursory phenomena nor crossover transients are seen for this type.

V. TWO-DIMENSIONAL-MAP MODEL

By the analog circuit simulation we have confirmed that symmetry-recovering crises exist for Eq. (10) as predicted by the one-dimensional-map model. However, the waveforms at the three types of crises were very different from that for the one-dimensional map. In this sec-

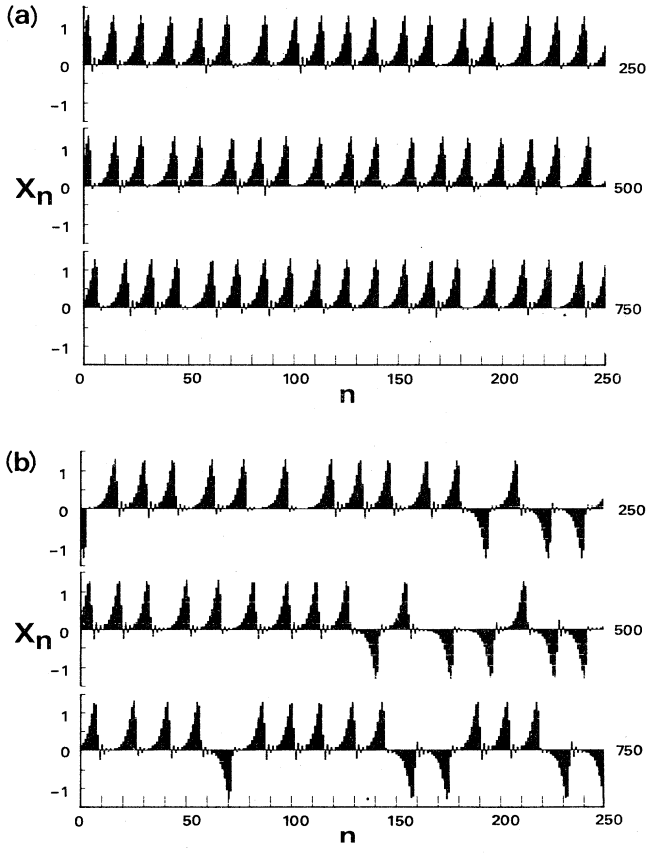

FIG. 8. Calculated waveforms (a) before and (b) after the type I crisis. Graph of X_n of Eq. (15) for 750 iterations after preiteration. Parameters: $\alpha=0.1$, (a) $\mu=10.24$; (b) $\mu=10.30$.

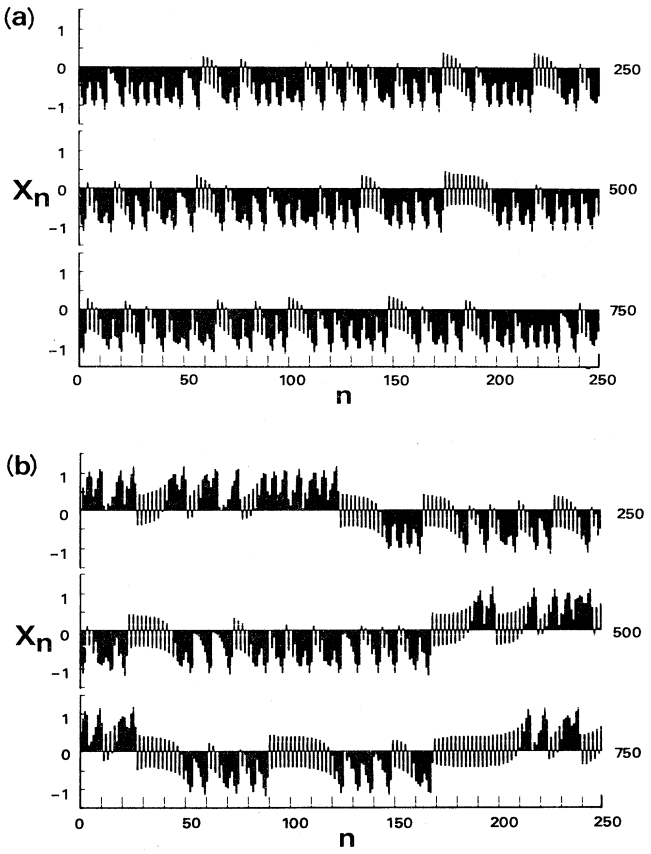

FIG. 9. Calculated waveforms (a) before and (b) after the type II crisis. Parameters: $\alpha=0.5$, (a) $\mu=3.54$; (b) $\mu=3.57$.

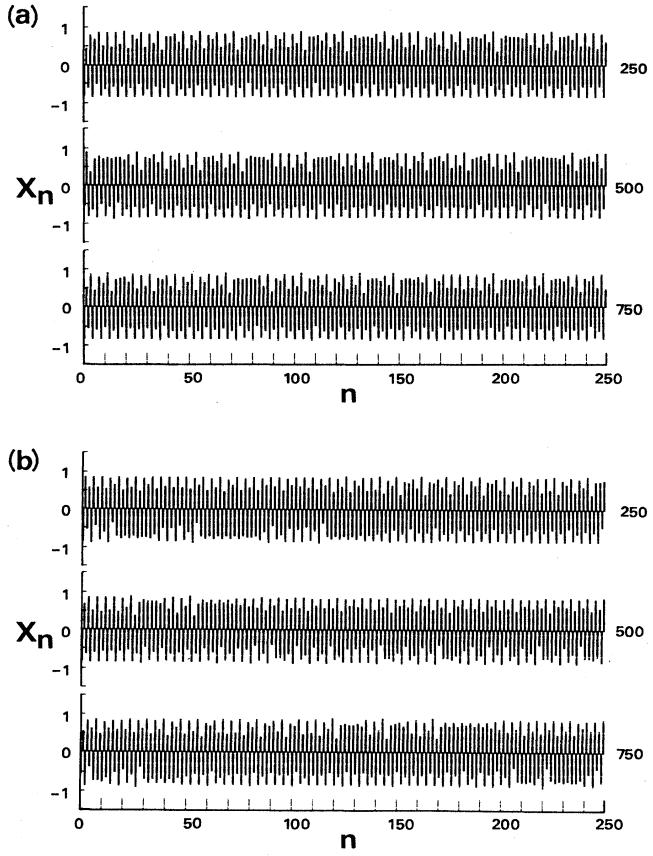

FIG. 10. Calculated waveforms (a) before and (b) after the type III crisis. Parameters: $\alpha=0.85$, (a) $\mu=2.944$; (b) $\mu=2.946$.

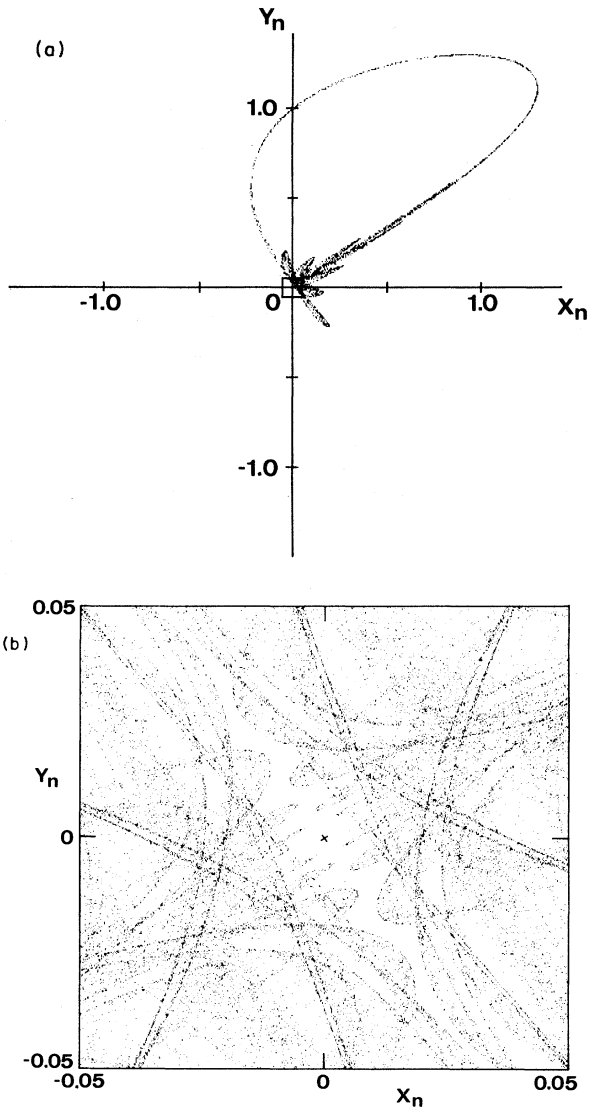

FIG. 11. (a) Chaotic attractor for Eq. (15) before the type I crisis. An initial point is chosen and its orbit is plotted after preiteration. The other coexisting attractor is obtained by the transformation $(X,Y)\rightarrow(-X,-Y)$. Parameters: $\alpha=0.1$, $\mu=10.24$. (b) Blowup of the boxed region in (a). Both coexisting attractors are plotted. A cross represents an unstable fixed point at (0,0). Parameters: $\alpha=0.1$, $\mu=10.244$.

tion we introduce a two-dimensional difference equation and show that the three types of crises occur for the equation with appropriate values of parameters.

We formally discretize Eq. (10) as

$$\gamma^{-1}\frac{X_{n+1}-X_n}{\Delta t}=-X_n+\mu F(X_{n-N})\ , \tag{13}$$

where N is an integer, $\Delta t=t_R/N$, $X_n=X(n\Delta t)$, and $F(X)=X(1-X^2)$. By introducing a parameter $\alpha=\gamma\Delta t$, we obtain the following $(N+1)$-dimensional difference equation:

$$X_{n+1}=(1-\alpha)X_n+\alpha\mu F(X_{n-N})\ . \tag{14}$$

In the limit $\alpha\rightarrow 0$, N and $t_R=$const, Eq. (14) approximates the differential equation (10) with $t_R=0$. For the case $\alpha=1$, Eq. (14) reduces to the one-dimensional difference equation (11). So α is a parameter which connects a difference equation and a differential equation as $t_R\gamma$ does in Eq. (10).

Here we crudely set $N=1$ in Eq. (14) and obtain a two-dimensional difference equation:[15]

$$X_{n+1}=(1-\alpha)X_n+\alpha\mu F(Y_n)\ , \tag{15a}$$

$$Y_{n+1}=X_n\ , \tag{15b}$$

where $Y_n=X_{n-1}$. The equation is invariant under the transformation $(X,Y)\rightarrow(-X,-Y)$.

Surprisingly, we could find the three types of crises in this oversimplified equation. In Figs. 8, 9, and 10 we show the waveforms near the crises. The clear correspondences to Figs. 5, 6, and 7 are seen. In particular, the same precursors and crossover transients appear for types I and II. Type I was found for smaller values of α (near the differential equation limit), type III was found for $\alpha\lesssim 1$ (near the difference equation limit), and type II was in the middle. The order is consistent with the results in Sec. IV.

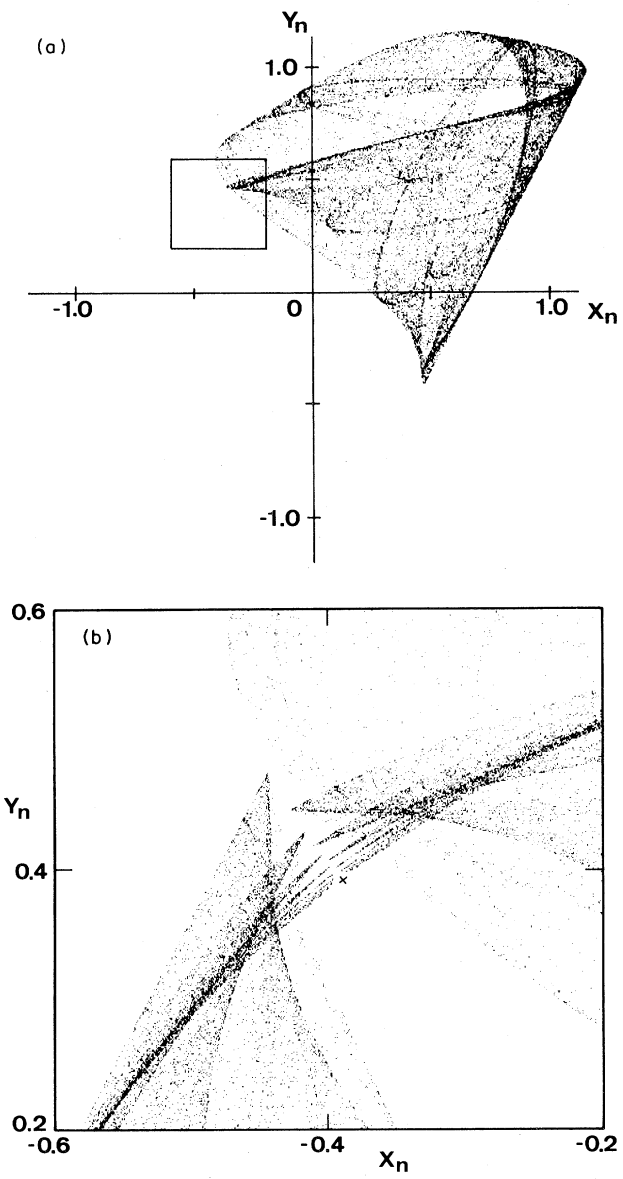

FIG. 12. (a) Chaotic attractor for Eq. (15) before the type II crisis. The other coexisting attractor is obtained by the transformation $(X,Y)\rightarrow(-X,-Y)$. Parameters: $\alpha=0.5$, $\mu=3.51$. (b) Blowup of the boxed region in (a). Both coexisting attractors are plotted. Parameter μ is closer to $\mu_{(0)}$ than in (a). A cross represents one of unstable period-2 points at $(\pm 0.39,\mp 0.39)$. Parameters: $\alpha=0.5$, $\mu=3.541$.

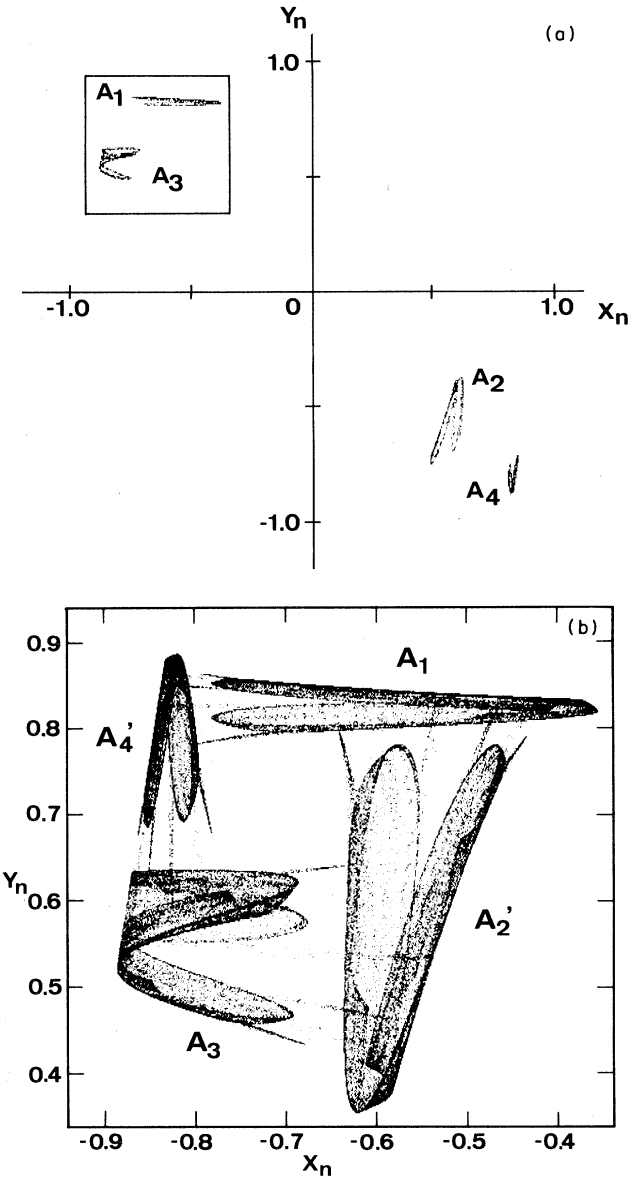

FIG. 13. Four-piece chaotic attractor (A_2,A_2,A_3,A_4) for Eq. (15) before the type III crisis. The other coexisting attractor (A_1',A_2',A_3',A_4') is obtained by the transformation $(X,Y)\rightarrow(-X,-Y)$. Parameters: $\alpha=0.85$, $\mu=2.93$. (b) Blowup of the boxed region in (a). Parameter μ is above the critical value for the crisis; therefore, attractor pieces are merged to form a two-piece attractor. Parameters: $\alpha=0.5$, $\mu=2.946$.

As described in Sec. III, for the one-dimensional map the symmetry crisis is undergone when a strange attractor collides with an unstable fixed point and the other strange attractor. Here we investigate the situation for the two-dimensional cases. Figures 11, 12, and 13 show the strange attractors near the crises of type I, II and III, respectively.

Type I. Figure 11(a) shows the strange attractor just before the crisis. The other coexisting attractor is obtained by the transformation $(X,Y)\rightarrow(-X,-Y)$. The two limit-cycle–like attractors are about to touch each other near the origin. A round trip of the cycle forms a pulse in Fig. 8. At $\mu=\mu_{(0)}$, two attractors are merged and for $\mu\lesssim\mu_{(0)}$, an orbit on an attractor can go over to the other attractor.

Figure 11(b) is an enlargement of part of Fig. 11(a). The two attractors are clearly separated. The regular structure of the attractors is a reflection of the existence of a fixed point (0,0) of Eq. (15). By the stability analysis, we can see that the eigenvalues ρ_1,ρ_2 of the linearized map

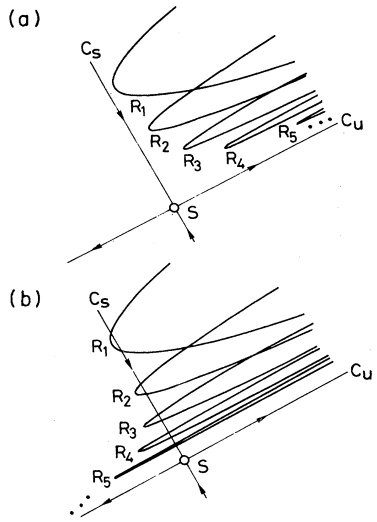

FIG. 14. Schematic illustration for crisis of a chaotic attractor through a saddle point S. (a) Before and (b) after the crisis, the regions R_i are mapped to R_{i+1}. C_s and C_u represent the stable and unstable invariant curves of S, respectively.

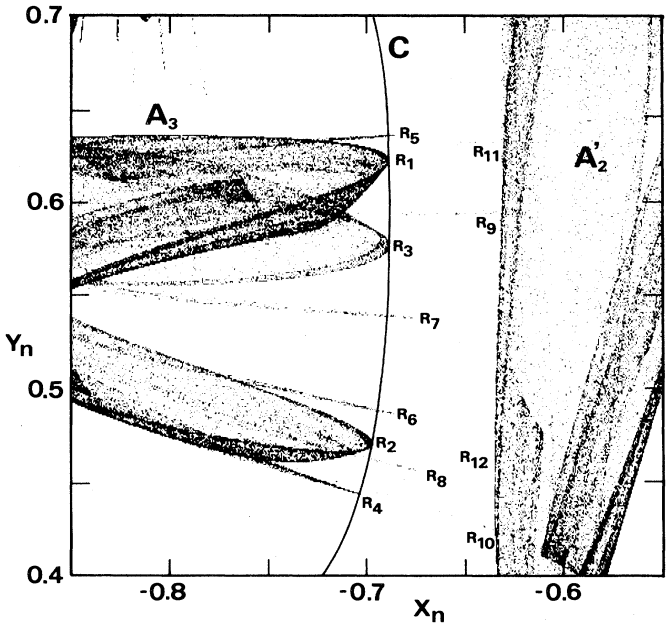

FIG. 15. Blowup of part between A_3 and A'_2 of Fig. 13(b). Parameter μ is above $\mu_{(0)}$. The regions R_i are mapped to R_{i+1} by $T^{(4)}$. C represents an unstable invariant curve. Parameters: $\alpha=0.85$, $\mu=2.2447$.

at (0,0) satisfy the following relations: $-1<\rho_1=-0.66<0$, $1<\rho_2=1.56$. The corresponding eigenvectors are $\vec{u}_1=-0.66\hat{x}+\hat{y}$, $\vec{u}_2=1.56\hat{x}+\hat{y}$. According to the classification of the fixed points in the Appendix, the point (0,0) is DR^1 for this parameter value. To simplify the situation, we consider a composite map $T^{(2)}=T\circ T$, where T is a map defined by Eq. (15). The point is a saddle (D^2) for $T^{(2)}$ since $0<\rho_1^2<1<\rho_2^2$. We use schematic illustrations in Fig. 14 to give general discussions. The point S is a saddle, and C_s and C_u are the stable and unstable invariant curves, respectively. The eigenvectors $\vec{u}_1$ and $\vec{u}_2$ are tangent to C_s and C_u at S. When $\mu<\mu_{(0)}$ [Fig. 14(a)], C_s is also the boundary separating the basins of attraction for the two attractors. The region R_1, which is mapped from somewhere in the attractor, is mapped to $R_2, R_3, \ldots$, successively, and at last repelled back along C_u. When the crisis is reached, R_1 touches the boundary C_s; as a result, R_i ($i=2,3,\ldots$) touches C_s and R_∞ touches S. As seen in Fig. 14(b), for $\mu\gtrsim\mu_{(0)}$, points in R_1 over C_s are repelled over to the other attractors along C_u after some iterations of the map.

Near the crisis, a point mapped close to C_s in R_1 will need many iterations to be repelled away from S, namely, the orbit is trapped to S temporarily. If S is a period-n point (a fixed point for $T^{(n)}$), one will observe n-periodic oscillation with some duration. Such phenomena will be seen as a precursor of crisis when $\mu\lesssim\mu_{(0)}$ and as a crossover transient when $\mu\gtrsim\mu_{(0)}$.

Type II. A wide-spread attractor is seen in Fig. 12(a). The other coexisting attractor lies symmetrically. The touch occurs near period-2 points ($\pm0.39,\mp0.39$), whose stability is D^2. Figure 12(b) shows a blowup where we see the same structure as in Fig. 14(a). We can hardly see the regular structure in Fig. 12(a) because μ is not as close to $\mu_{(0)}$. The bursts of oscillation seen in Fig. 9 mean that the orbit is trapped to the period-2 points. The closer the point is dropped to the stable invariant curve, the longer the regular oscillation continues.

Type III. The situation is rather more complicated than in types I and II. Before the crisis, two four-piece strange attractors are coexisting. In Fig. 13(a), only the attractor (A_1,A_2,A_3,A_4) is pictured. The other attractor (A'_1,A'_2,A'_3,A'_4) is obtained by the transformation $(X,Y)\to(-X,-Y)$. An orbit cycles as $A_1\to A_2\to A_3\to A_4\to A_1$ or as $A'_1\to A'_2\to A'_3\to A'_4\to A'_1$, and gives period-4 chaos as in Fig. 10(a). The flat boundary in the waveform comes from the fact that the attractor pieces A_4 and A'_4 have narrower width in the X direction than the other pieces.

After the crisis occurs, the two attractors are merged as seen in Fig. 13(b). To see how the merging occurs, a further blowup is given in Fig. 15. Between A_3 and A'_2 there exists an invariant curve C, which forms a part of the basin boundary before the crisis. We can see that the regions R_i ($i=1,2,\ldots$) are mapped to R_{i+1} by $T^{(4)}$. In the course of iterations of the map, the regions are stretched in the direction across the curve C, and their tips are attracted to A'_2. The regions R_i ($i>12$) can't be seen for the points are so dispersed by the stretching.

The configuration of R_i along C can be understood as follows. Restriction $T^{(4)}$ to the invariant curve C gives a one-dimensional unimodal map which exhibits period-2 chaos. So the configuration of R_i is somewhat erratic, although we can group them into (R_{2n-1}) and (R_{2n}) $(n=1,2,\ldots)$.

It is seen, from the theory of the unimodal map, that there exist infinite numbers of unstable fixed points on C; one UR^4, two UR^8, four UR^{16}, ... Therefore, we may

say that the crisis occurs through UR^k ($k=2n$, $n=0,1,2,\ldots$). Here, however, we are tempted to modify Grebogi's definition of crises as "a collision of a chaotic attractor to the basin boundary."

VI. CONCLUSION

In summary, we have investigated the symmetry-recovering crises of chaos in a polarization-related optically bistable system. Through the crises, chaotic states having the polarization asymmetry, which is inherited from the first bifurcation, jump back to a symmetric state. We have found three distinct types of the crises by changing the parameter $t_R\gamma$. All of the waveforms near these crises are very different from that for the one-dimensional-map model which has been used to analyze difference-differential equations such as Eq. (10), whereas a two-dimensional-map model we introduced gives good qualitative explanations to the three types of crises.

As Grebogi *et al.*[13] said, crises occur when a chaotic attractor collides with an unstable fixed point or an unstable periodic orbit. In our cases of types I, II, and III, collisions to the unstable fixed points of types DR^1, D^2, and UR^{4k} ($k=2^n$) occur. For types I and II the unstable fixed fixed point has a stable invariant curve in addition to an unstable invariant curve. The stable curve forms a part of the basin boundary which separates the paired chaotic attractors before the crisis. Along the stable invariant curve, regular structures are formed just before and after the crisis. For type III, a one-dimensional map on the invariant curve, which yields chaos, gives marked structure to the strange attractors near the crisis.

Perhaps there exist other types of symmetry-recovering crises than those we treated here. [For example, Fig. 3(c) in Ref. 16 suggests another type which is close to type III.] Some of them may need models in higher dimensions. Even for such cases, types of the unstable fixed point will characterize the crises. Statistical behavior near each crisis such as in Eq. (12) should be investigated.

Finally, we estimate experimental parameters to observe the phenomena in an all-optical system. The Na system of Ref. 12 with which we have observed the symmetry-breaking bifurcation should be modified. The delay t_R can be provided by an optical fiber with sufficient length L. We see from Eq. (10) and the requirement $t_R\gamma \gtrsim 1$ that the required power density I_0 is inversely proportional to t_R or L. For $L=1$ km ($t_R=6$ μs), I_0 is estimated to be $1\sim 10$ W/mm^2, which is not an unrealistic value considering the use of a multimode laser.

ACKNOWLEDGMENTS

This research was supported by the Ministry of Education, Science, and Culture in Japan, under a Grant-in-Aid for Scientific Research. One of us (M.K.) is a recipient of a Sakkokai Foundation Fellowship.

APPENDIX: CLASSIFICATION OF A FIXED POINT

The stability of a fixed point of a two-dimensional map T can be characterized by the eigenvalues ρ_1 and ρ_2 of the linearized map.[15] If $|\rho_1|\neq 1$ and $|\rho_2|\neq 1$, the fixed point is called simple. A fixed point is called orientation preserving when $\rho_1\rho_2>0$ and orientation reversing when $\rho_1\rho_2<0$. Orientation-preserving simple fixed points are classified as follows: completely stable (S), $|\rho_1|<1$, $|\rho_2|<1$; completely unstable (U), $|\rho_1|>1$, $|\rho_2|>1$; directly unstable (D), $0<\rho_1<1<\rho_2$; inversely unstable (I), $\rho_1<-1<\rho_2<0$. The orientation reversing one is classified as follows: completely stable (SR), $|\rho_1|<1$, $|\rho_2|<1$; completely unstable (UR), $\rho_1<-1$, $\rho_2>1$; directly unstable (DR), $-1<\rho_1<0$, $1<\rho_2$; inversely unstable (IR), $\rho_1<-1$, $0<\rho_2<1$. We can extend the above notation to n-periodic points; namely, if an n-periodic point P is a fixed point DR of the map $T^{(n)}$, for example, we then denote P as DR^n.

[1]K. Ikeda, Opt. Commun. 30, 257 (1979); K. Ikeda, H. Daido, and O. Akimoto, Phys. Rev. Lett. 45, 709 (1980).

[2]K. Ikeda and O. Akimoto, Phys. Rev. Lett. 48, 617 (1982); K. Ikeda, K. Kondo, and O. Akimoto, *ibid.* 49, 1467 (1982).

[3]H. M. Gibbs, F. A. Hopf, D. L. Kaplan, and R. L. Shoemaker, Phys. Rev. Lett. 46, 474 (1981); F. A. Hopf, D. L. Kaplan, H. M. Gibbs, and R. L. Shoemaker, Phys. Rev. A 25, 2172 (1982); M. W. Derstein, H. M. Gibbs, F. A. Hopf, and D. L. Kaplan, *ibid.* 26, 3720 (1982); M. W. Derstein, H. M. Gibbs, F. A. Hopf, and D. L. Kaplan, *ibid.* 27, 3200 (1983).

[4]H. J. Carmichael, C. M. Savage, and D. F. Walls, Phys. Rev. Lett. 50, 163 (1983); H. J. Carmichael, in *Laser Physics, Lecture Notes in Physics 182,* edited by J. D. Harvey and D. F. Walls (Springer, Berlin, 1983), p. 64.

[5]H. Nakatsuka, S. Asaka, H. Itoh, K. Ikeda, and M. Matsuoka, Phys. Rev. Lett. 50, 109 (1983).

[6]T. Poston, D. F. Walls, and P. Zoller, Opt. Acta 29, 1691 (1982).

[7]J. V. Moloney and H. M. Gibbs, Phys. Rev. Lett. 48, 1607 (1982); D. W. McLaughlin, J. V. Moloney, and A. C. Newell, *ibid.* 51, 75 (1983).

[8]M. Kitano, T. Yabuzaki, and T. Ogawa, Phys. Rev. Lett. 46, 926 (1981); Phys. Rev. A 24, 3156 (1981).

[9]C. M. Savage, H. J. Carmichael, and D. F. Walls, Opt. Commun. 42, 211 (1982); F. T. Arecchi, J. Kurmann, and A. Politi, *ibid.* 44, 421 (1983).

[10]S. Cecchi, G. Giusfredi, E. Petriella, and P. Salieri, Phys. Rev. Lett. 49, 1928 (1982); F. Mitschke, J. Mlynek, and W. Lange, *ibid.* 50, 1660 (1983); W. J. Sandle and M. W. Hamilton, in *Laser Physics, Lecture Notes in Physics 182,* edited by J. D. Harvey and D. F. Walls (Springer, Berlin, 1983), p. 54.

[11]T. Yabuzaki, M. Kitano, and T. Ogawa, *Proceedings of Lasers '82, New Orleans* edited by R. Powell (STS, McLean, Virgina, 1983).

[12]T. Yabuzaki, T. Okamoto, M. Kitano, and T. Ogawa (unpublished).

[13]C. Grebogi, E. Otto, and J. A. York, Physica 7D, 181 (1983); Phys. Rev. Lett. 48, 1507 (1982).

[14]M. Kitano, T. Yabuzaki, and T. Ogawa, Phys. Rev. Lett. 50, 713 (1983).

[15]Various kinds of strange attractors for this equation are presented by H. Kawakami, Kokyuroku 370, 88 (1979).

[16]F. T. Arecchi and F. Lisi, Phys. Rev. Lett. 49, 94 (1982).